IOP Conf. Series: Journal of Physics: Conf. Series **830** (2017) 012126 doi:10.1088/1742-6596/830/1/012126

OpenMP parallel computing of 2D TiC combustion synthesis process using an explicit finite-volume scheme

A Aoufi

Centre SMS, Laboratoire Georges Friedel, UMR CNRS 5307, EMSE, 158 cours Fauriel, 42023 Saint-Etienne. France

E-mail: aoufi@emse.fr

Abstract. This paper analyzes from a numerical point of view the ignition and propagation of the combustion front during the exothermic TiC combustion synthesis of a material made of pressed titanium and carbide particles when thermophysical properties are either assumed constant or temperature and conversion rate dependent. A two-dimensional cylindrical geometry is considered. The heat supply is prescribed on one, two or three sides of the physical domain. A one-step kinetics is used to describe the reaction Ti+C→TiC in a solid phase and leads to the computation of the conversion rate. A coupling with a non-linear heat equation which takes into account the heat generated by the exothermic kinetics and the two allotropic phase-changes is considered. An explicit finite-volume discretization of the coupled system is constructed and analyzed. Time-step's stability condition is given for a general expression of the thermo-physical characteristics. A discrete maximum principle is reported. Open MP API was used to parallelize the numerical software written in C. An average speedup of three was obtained on an intel quad-core processor i7-2600. The ignition time and the fraction of unreacted material are systematically computed and compared for several heat supply scenario.

1. Introduction

The present paper is devoted to the numerical computation of TiC combustion synthesis [1,2] in a 2D cylindrical coordinate system using an explicit scheme implemented on a multicore architecture using OpenMP API. It is organized as follows. Section two reports the main features of the mathematical modelling of this combustion synthesis process (coupling a partial differential equation with a differential equation) and the expression used for thermophysical parameters (thermal conductivity and heat capacity). Section three outlines the explicit finite-volume discretization of both equations and reports a discrete maximum principle for both equations. Section four explains the main ingredients of the parallelization strategy based upon inserting OpenMP #pragma directives and analyzes the efficiency of the software on a multicore intel i7-2600 cpu. Section five presents some numerical simulation results used to systematically investigate the evolution of ignition curves when thermophysical properties are either constant or temperature and conversion rate dependent. The stability of the combustion wave is investigated thanks to the Zeldovitch number. The contribution of allotropic phase changes is also taken into account numerically. The effect of heat supply on one, two and three faces of the cylinder is also reported. A conclusion summarizes the results presented in this study.

2. Mathematical modeling

Temperature T in K, and conversion rate $\xi \in [0,1]$ are the key variables used to describe the evolution of the exothermic equation Ti+C →TiC. The mathematical modeling couples the enthalpy balance with a differential equation.

2.1. Nonlinear reaction diffusion and boundary condition

An enthalpy balance written for a cylinder Ω with radius *R* and height *H*, leads to the following non-linear reaction-diffusion equation

$$\rho Cp(T,\xi)\frac{\partial T}{\partial t} - \nabla.(\lambda(T,\xi)\nabla \mathrm{T}) = \rho \Delta H k(T)(1-\xi). \quad (1)$$

Along the symmetry axis of the cylinder, the adiabatic boundary condition is prescribed

$$\forall z \in [0,H], \quad -\lambda(T,\xi)\frac{\partial T}{\partial n}(0,z) = 0. \quad (2)$$

Radiative boundary conditions are defined for the three remaining subparts Γ of ∂Ω. The value of $T\infty,\Gamma$ ranges from 300 K (room temperature) to 2400 K. ϵ is the emissivity of the material and σ is the Stefan-Boltzmann constant.

$$-\lambda(T,\xi)\frac{\partial T}{\partial n} = \epsilon\sigma\left(T^4 - T_{\infty,\Gamma}^4\right) \quad (3)$$

The initial condition states that the sample is at room temperature T0 such that

$$\forall x \in \Omega, \quad T(x,0) = T_0 \quad (4)$$

2.2. Heat capacity

Assuming that the mass of the system remains constant, a linear mixing law between the heat capacity of reactants *Cp*Ti(*T*), *Cp*C(*T*) [3] and the heat capacity of the product *Cp*TiC (*T*) [3] weighted by the conversion rate of the reaction gives (Figure 1)

$$\mathrm{Cp}(T,\xi) = \xi.C_{P_{TiC}}(T,\xi) + (1-\xi).\frac{M_{Ti}.C_{P_{Ti}}(T)+M_C.C_{P_C}(T)}{M_{TiC}} \quad (5)$$

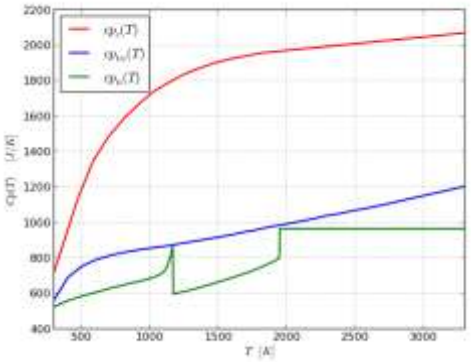

Figure1. Evolution of cptic(T), cpti(T) and cpc(T).

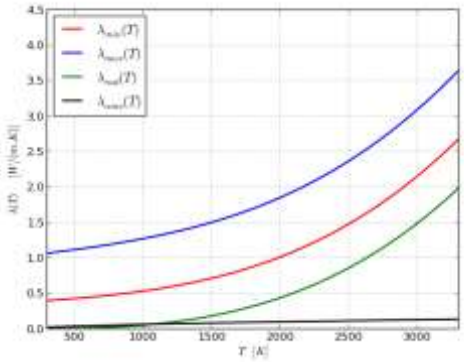

Figure2. Evolution of λ min(T), λ max(T), λ rad(T) and λ conv(T).

2.3. Thermal conductivity

The effective thermal conductivity of Ti+C power mixture is the sum of terms taken from [4],[5],[6]. $f_{sl} \in [0,1]$ is the liquid fraction at allotropic phase change occurring at $T_f = 1950$K. Figure (2) shows the range in which $\lambda(T,\xi,f_{sl})$ varies while omitting $\lambda_{fus}(f_{sl})$ defined only $T = T_f$.

$$\lambda\,(T,\,\xi,\,f_{sl}) = \lambda_{cond}\,(T,\xi,f_{sl}) + \lambda_{fus}\,(f_{sl}) + \lambda_{rad}\,(T\,) + \lambda_{conv}\,(T\,) \quad (6)$$

2.4. Kinetics

A first order kinetics with an Arrhenius equation for the rate constant describes Ti+C →TiC. It is given by

$$\frac{d\xi(x,t)}{dt} = k\big(T(x,t)\big)\big(1-\xi(x,t)\big),\ \ k(T) = k_0 e^{-\frac{E^*}{RT(x,t)}},\ \ \xi(x,0) = 0. \tag{7}$$

2.5. Analysis of the numerical simulations

The following three quantities are systematically computed in order to investigate the results of the numerical simulations presented in next sections:

- the synthesis temperature *Tsyn*(*x*) ($x \in \Omega$) is the weighted mean of the temperature by the kinetics defined (from [7]) by

$$\forall x \in \Omega, \qquad T_{syn}(x) = \int_0^{+\infty} T(x,t)\,\frac{d\xi}{dt}(x,t)dt \tag{8}$$

- the normalized fraction of unreacted material *nfum(t)* is defined (from [8])

$$\forall t > 0,\ \ nfum(t) = \frac{\|1-\xi(.,t)\|_{L^2(\Omega)}}{\|1\|_{L^2(\Omega)}} \in [0,1\,]. \tag{9}$$

- the maximum of the temperature *Tmax*(*t*) and the mean temperature $\bar{T}(t)$ of *T* (., *t*) over Ω are computed at each time *t* > 0.

3. Finite-volume discretization

The computational domain Ω is decomposed into a set of *NI*× *NJ* rectangular control volumes Ω*i,j* with "mass" *mi,j* . A conservative finite-volume cell-centered approximation is used to discretize the governing equations of the modeling. The handling of each phase change transition during which a liquid fraction appears is done thanks to a specific procedure.

3.1. Explicit finite-volume discretization of the reaction-diffusion equation

The integration of equation (1) over a space-time finite volume Ω*i,j* × [*tn*, *tn*+1] leads to the discrete equation, where $T_{i,j}^n$ is the mean of T over Ωi,j evaluated at tn

$$\begin{aligned} &m_{i,j}\rho C_p\big(T_{i,j}^n, \xi_{i,j}^n\big)\tfrac{T_{i,j}^{n+1}-T_{i,j}^n}{\Delta t} = E_{i,j}^n\big(T_{i+1,j}^n - T_{i,j}^n\big) - W_{i,j}^n\big(T_{i,j}^n - T_{i-1,j}^n\big) \\ &+N_{i,j}^n\big(T_{i,j+1}^n - T_{i,j}^n\big) - S_{i,j}^n\big(T_{i,j}^n - T_{i,j-1}^n\big) + m_{i,j}\rho\Delta H k\big(T_{i,j}^n\big)\big(1-\xi_{i,j}^n\big). \end{aligned} \tag{10}$$

Similar discrete equations are written for control volumes intersecting the boundary ∂Ω. Let us define Δt_{rd}^{stab} by

$$\Delta t_{rd}^{stab} = \min_{i,j}\left(\frac{m_{i,j}\rho C_p\big(T_{i,j}^n,\xi_{i,j}^n\big)}{E_{i,j}^n+W_{i,j}^n+N_{i,j}^n+S_{i,j}^n}\right). \tag{11}$$

Under the assumption that $0 < \Delta t \leq \Delta t stab$, the following discrete maximum principle properties for the time-explicit discretization ([7],[9] for the time-implicit discretization) are established by induction

(i) $\forall (i,j) \in [1, NX] \times [1, NY]: 0 < T_0 \leq T_{i,j}^n \Longrightarrow 0 < T_0 \leq T_{i,j}^{n+1}$.

(ii) $\forall (i,j) \in]1, NX[\times]1, NY[: T_{i,j}^{n+1} \leq T_{i,j}^n + \Delta t\,\frac{k_0 \Delta H}{C_p^{min}}$, where $C_p^{min} = \min_{T>0,\xi\in[0,1]} C_p(T,\xi)$.

It is worth mentioning that when the thermo-physical properties are constant, the time-step for the reaction-diffusion is also constant, therefore the stability condition Δt_{rd}^{stab} is computed once and passed as a parameter to the function advancing the heat transfer the case. When these parameters are temperature and conversion rate dependent, Δt_{rd}^{stab} is recomputed at each step once the positive quantities $E_{i,j}^n, W_{i,j}^n, N_{i,j}^n, S_{i,j}^n$ are evaluated as a function of T and ξ. The computational complexity is therefore a multiple of $NI \times NJ$.

3.2. Explicit finite-volume discretization of the differential equation

The integration of equation (7) over a space-time finite volume leads to the discrete equation

$$\xi_{i,j}^{n+1} - \xi_{i,j}^n = \Delta t k\big(T_{i,j}^n\big)\big(1-\xi_{i,j}^n\big). \tag{12}$$

Let us define $\Delta t_{kin}^{stab} = \min_{i,j}\frac{1}{k\left(T_{i,j}^n\right)}$. Under the assumption that $0 < \Delta t \leq \Delta t_{kin}^{stab}$, the following discrete maximum principle properties ([7],[9] for the time-implicit discretization) are established by

induction for $(i,j) \in [1,NX] \times [1,NY]$

(i) $0 \leq \xi_{i,j}^n \leq 1 \Longrightarrow 0 \leq \xi_{i,j}^{n+1} \leq 1.$

(ii) $0 \leq \xi_{i,j}^n \leq \xi_{i,j}^{n+1}.$

3.3. Choice of the time-step

The time-step Δtn is computed thanks to the expression

$$\Delta t_n = \left(\Delta t_{rd}^{stab}, \Delta t_{kin}^{stab}\right). \quad (13)$$

It is worth mentioning that in the numerical simulations presented in next sections, we always observed that $\Delta t_{rd}^{stab} < \Delta t_{kin}^{stab}$. This is explained by the small value of the activation energy E^*.

4. Parallel computing using OpenMP

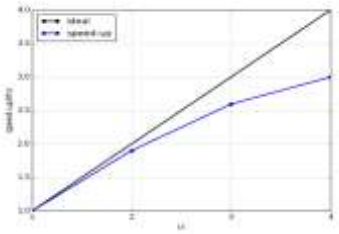

Figure 3. Evolution of speed-up $s_{th} = t(1)/t(th)$, for th=1,…,4.

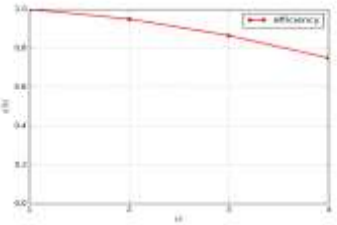

Figure 4. Evolution of efficiency $e_{th} = s_{th}/th$, for th=1,…,4.

The numerical scheme is implemented in C using our library Hepha¨ıstos, compiled wit gnu gcc compiler (version 4.8.2) and run under Ubuntu 14.04 (64 bits) OS. Two dimensional arrays are converted to single dimensional arrays. All loops are parallelized thanks to OpenMP directives manually inserted into the code. Highest level of optimisation activated by an adequate compiler flag is chosen for gcc compiler. This leads to the vectorization of loops using SIMD units of the intel i7-2600 multicore processor.

The value of the time-step for the reaction-diffusion equation is either computed once at the beginning of the program (the values of λ and Cp are constant) or dynamically determined by a reduction operation (the values of λ and Cp are temperature and conversion rate dependent). The efficiency of the program is increased by avoiding redundant computations. All loop invariant quantities are computed once and stored into arrays. Trivial nested loops are parallelized with a specific openmp #pragma directive. The numerical results are checked and are independent from the number of cores. Figure 3 shows the scalability of the numerical code. A speedup of 3 was obtained when the number of threads is 4 for a given mesh. It varies slightly as a function of the mesh. Figure 4 shows that the efficiency of the numerical code is above 0.75 when four cores are used. This means that time spent on transferring datas between cores is much lower than time spent on computations. The implementation is therefore efficient.

5. Numerical simulation

5.1. Stability analysis of the combustion front

Linear stability analysis (from [10]) is based upon the computation of Zeldovich number $Ze = \frac{E^*(T_{ad}-T_0)}{RT_{ad}^2}$. Here $T_{ad} \cong 2900K$ and $E^* \cong 30kcal = 125.4$ kJ, then $Ze = 4.52 < 2\left(2+\sqrt{5}\right) \cong 8.4723$ for which a stable propagation with a constant velocity is obtained.

5.2. Key simulation parameters

A simulation is characterized by (*Tz*=0, *Tr*=*R*, *Tz*=*H*) and stopped when *nfum*(*t*) < 10−2, hence the cooling of the material down to room temperature is not computed. *R* = 0.5cm and *H* =1 cm. The spatial distribution of *Tsyn*(*x*) is systematically determined for *T* =1600 K when a) constant properties

(c-pc-0), b) variables properties without phase change (v-pc-0) or c) variables properties with phase change (v-pc-1) are considered.

5.3. Propagation of a longitudinal front

In this case, (*Tz*=0, *Tr*=*R*, *Tz*=*H*) = (*Tf* , 300, 300), where *Tf* =800, 1600, 2400. A uniform tensorial grid made of 32 × 512 cells is used for the computations. Results are presented in Figure 5, Figure 6, Figure 7 and show that nonlinear expression for $Cp(T,\xi)$ and $\lambda(T,\xi)$ have a leading contribution to the celerity of the synthesis.

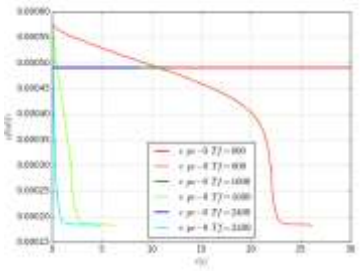

Figure 5. Time evolution of $\Delta t_{rd}^{stab}(t)$

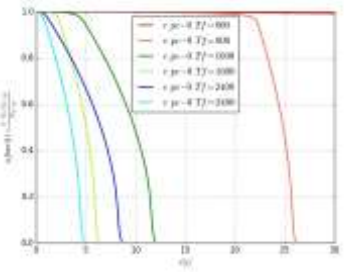

Figure 6. Time evolution of Nfum (t)

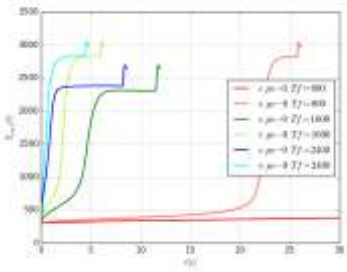

Figure 7. Time evolution of Tmax (t)

5.4. Propagation of a converging radial front

In this case, (*Tz*=0, *Tr*=*R*, *Tz*=*H*) = (300, *Tf* , 300), where *Tf* =800 K, 1600 K, 2400 K. A uniform tensorial grid made of 512 × 32 cells is used for the computations. Results are presented in Figure 8, Figure 9, Figure 10, Figure 11, Figure 12. A conclusion similar to the longitudinal case can be established. Phase changes contribution is noticeable graphically.

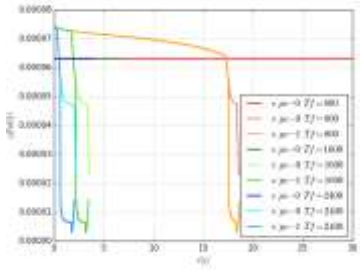

Figure 8. Time evolution of$\Delta t_{rd}^{stab}(t)$

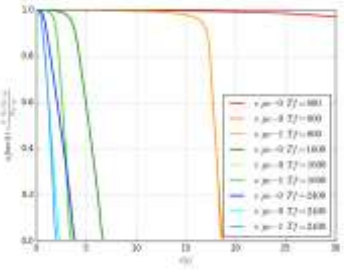

Figure 9. Time evolution of *nfum* (*t*)

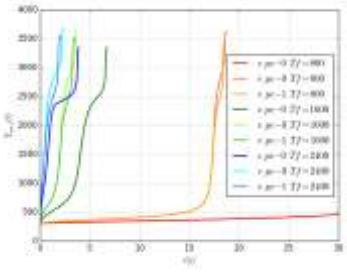

Figure 10. Time evolution of *Tmax* (*t*)

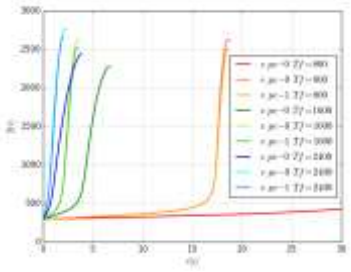

Figure 11. Time evolution of *T* (*t*)

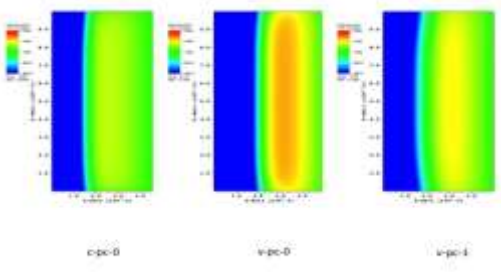

Figure12. Spatial distribution of *Tsyn*(*x)*

5.5. Propagation of two longitudinal fronts

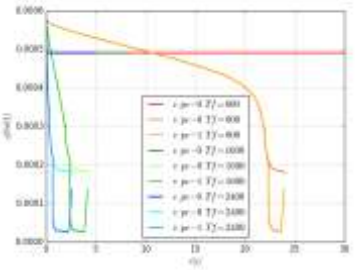

Figure 13. Time evolution of$\Delta t_{rd}^{stab}(t)$

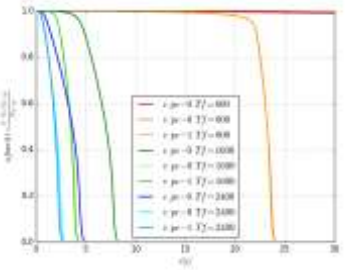

Figure 14. Time evolution of *nfum* (*t*)

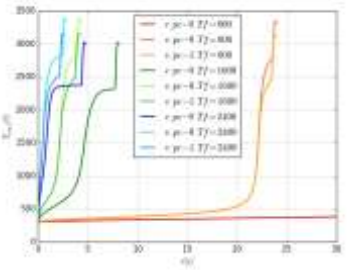

Figure 15. Time evolution of *Tmax* (*t*)

In this case, (*Tz*=0, *Tr*=*R*, *Tz*=*H*) = (*Tf* , 300, *Tf*), where *Tf* =800 K, 1600 K, 2400 *K*. A uniform tensorial grid made of 32 × 512 cells is used for the computations. Results are presented in Figure 13, Figure 14, Figure 15, Figure 16, Figure 17. A similar conclusion can be established. Moreover, along *z* = *H*/2 a melting might occur because *Tmax*(*t*) is locally greater than 3000 K. Latent heat of phase change is therefore needed to accurately capture the effects of this melting.

5.6. Propagation of three converging fronts

In this case, (*Tz*=0, *Tr*=*R*, *Tz*=*H*) = (*Tf*, *Tf*, *Tf*), where *Tf*=800, 1600, 2400. This corresponds to the practical case where the cylindrical sample is placed inside a furnace with uniform temperature *Tf* . A uniform tensorial grid made of 512 × 512 cells is used for the computations.

Results are presented in Figure 18, Figure 19, Figure 20, Figure 21, Figure 22 (notice the symmetries induced by the symmetries of the boundary conditions). The conclusion is similar to those previously obtained.

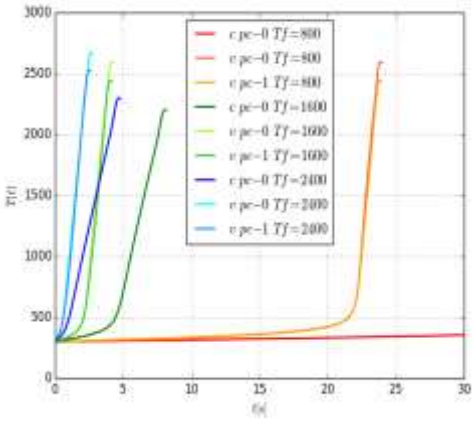

Figure 16. Evolution of $\overline{T}(t)$

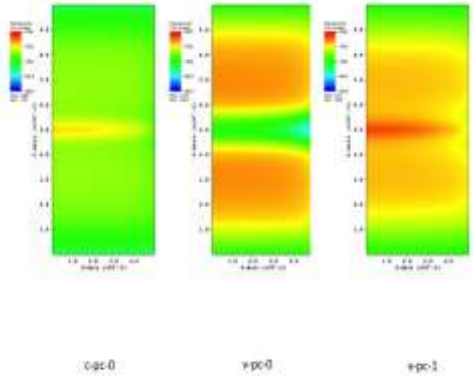

Figure 17. Spatial distribution of *Tsyn*(*x*)

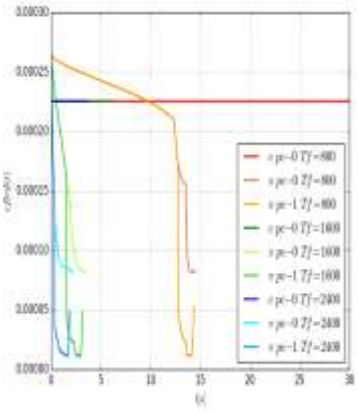

Figure 18. Time evolution of$\Delta t_{rd}^{stab}(t)$

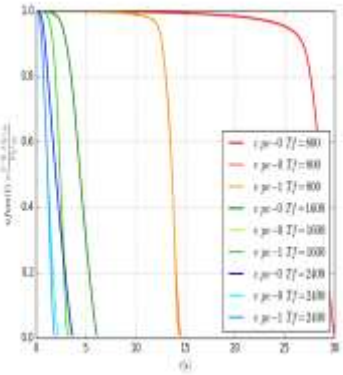

Figure 19. Time evolution of *nfum* (*t*)

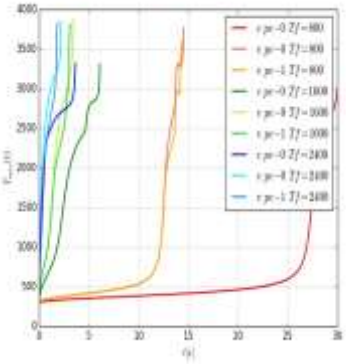

Figure 20. Time evolution of *Tmax* (*t*)

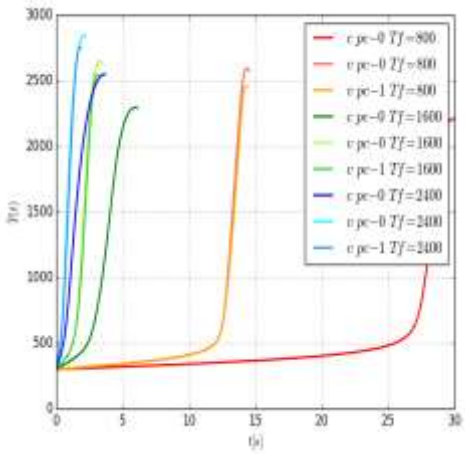

Figure 21. Evolution of $\overline{T}(t)$

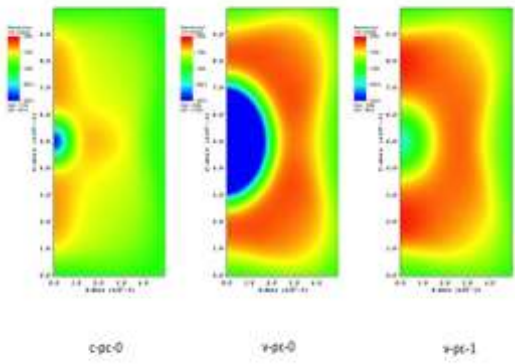

Figure 22. Spatial distribution of *Tsyn*(*x*)

—

5.7. Ignition curves

Figure 23, Figure 24 and Figure 25 show the ignition (instant τ such that *nfum*(τ)≅ 0.95) curves obtained respectively for two propagating fronts, three propagating fronts and one radially converging front as a function of furnace's temperature *Tf* . Each set of curves, presents a high dependence on *Cp*(*T*, ξ) and λ(*T*, ξ). The contribution of phase changes is negligible (<1%)

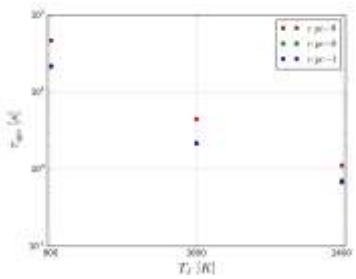

Figure 23. Ignition time for two travelling fronts

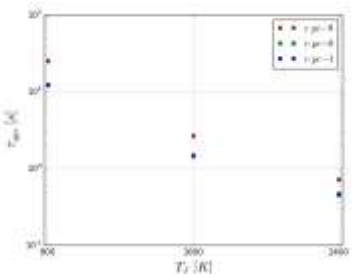

Figure 24. Ignition time for three travelling fronts

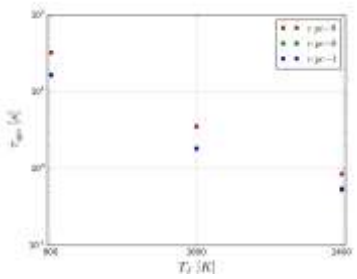

Figure 25. Ignition time for one radially travelling front

6. Conclusions and perspectives

In the present paper we have shown through numerical simulations (thanks to a tuned parallel software using OpenMP and implementing an explicit finite-volume scheme for which a discrete maximum principle was established) that independently of the way external heat supply is applied on part of the boundary $\partial\Omega$, the expressions used for $Cp(T, \xi)$ and $\lambda(T\,\xi)$ have a significant influence on TiC combustion synthesis process, quantified by $nfum(t)$ and $Tsyn(x)$. The contribution of the two allotropic phase changes ranges from negligible to minimal.

A similar approach is currently investigated in the case of a cubic sample where the computations are genuinely three dimensional.

References

[1] Merzhanov A G 1969 *Combustion and Flame* **13** pp 143-156
[2] Merzhanov A G 1994 Combustion Science and Technology **1994** pp 307-336
[3] Touloukian S and Dewitt D P 1972 *The TPRC Data Series* IFI Plenum **8**
[4] Vrel D, Lihrmann J M and Tobaly P 1994 *Journal of Materials Synthesis and Processing* **2** pp 179-187
[5] Wakao N and Kato K 1969 *Journal of Chemical Engineering of Japan* **2-1** 24-32
[6] Viljoen H J and Hlavacek V 1991 *AIChE J.* **37** pp 1595-1597
[7] Aoufi A and Dammame G 2006 *Applied Mathematics and Computation* **176** pp 99-116
[8] Aoufi A 2014 *Izvestia vizov physica* **57** pp 16-19
[9] Aoufi A 2004 *Integral Methods in Science and Engineering* Birkhauser, Basel pp 1-6
[10] Bayliss A and Matkowsky B J 1987 *JCP* **71-1** pp 147-168